# Enhancing Defects Characterization in Pulsed Thermography by Noise Reduction

[1,*]R. Marani, [2]D. Palumbo, [2]U. Galietti, [1]E. Stella, [1]T. D'Orazio

[1]*Institute of Intelligent Industrial Technologies and Systems for Advanced Manufacturing, National Research Council of Italy, via Amendola 122 D/O, Bari, Italy*

[2]*Department of Mechanics, Mathematics and Management, Politecnico di Bari, viale Japigia 182, Bari, Italy*

**corresponding author, e-mail: roberto.marani@stiima.cnr.it*

## Abstract

In the field of NDT techniques for aeronautic components of composite materials, the development of automatic and robust approaches for defect detection is largely desirable for both safety and economic reasons. This paper introduces a novel methodology for the automatic analysis of thermal signals resulting from the application of pulsed thermography. Input thermal decays are processed by a proper FIR filter designed to reduce the measurement noise, and then modeled to represent both sound regions and defective ones. Output signals are thus fitted on an exponential model, which approximates thermal contrasts with three robust parameters. These features feed a decision forest, trained to detect discontinuities and characterize their depths. Several experiments on actual sample laminates have proven the increase of the classification performance of the proposed approach with respect to related ones in terms of the reduction of missing predictions of defective classes.

## Keywords

Pulsed Thermography; FIR Filter; Model Approximation; Decision Forest.

## 1. Introduction

In the recent years, composite laminates have become the preferred materials for building large components in transportation industry because of their properties of lightweight, fatigue and corrosion resistance, capability to mold large complex shapes, high stability in space environment and so on. However, the susceptibility to impact-damage and the strong possibility of internal damage going unnoticed represent one of the weakness of this kind of materials. For this reason, non-destructive testing (NDT) techniques assume a key role for the analysis of internal defects both at the end of production processes and for maintenance checks.

From one side, a lot of efforts have been focused on the development of NDT techniques such as X-ray [1][2], ultrasound [3]-[5], shearography [6], vibration testing [7], electrical potential technique [8], infrared thermography [9],[10], and also their combinations aimed to gain more sensitivity. On the other side, few works can be found for the development of processing approaches designed to support decision processes targeted to the automatic evaluation of internal defects.

With reference to the aeronautic industry, ultrasonic C-scans have been used as standard NDT technique to assess the internal quality of large components made of composite materials [11]. Ultrasonic testing allows the determination of the depth of the defects with good accuracy. However, several inspections with different probes are required, thus increasing the cost of the testing phase [12]. For this reason, the use of both lock-in (LT) and pulsed thermography (PT) [13] is highly encouraged for the inspection of large areas

since these techniques do not require any coupling medium (easily adaptable also for maintenance checks) and the testing time is relatively short with respect to other techniques [14]-[16].

Recently, many signal processing algorithms have been applied to temperature signals in order to extract significant features, to enhance signals and to allow the detection of deep defects, even with high noise levels [17]-[19]. Researches have investigated also the use of machine learning techniques for developing automatic systems both for the detection and the characterization of different defects. These automatic systems can be used to support human operators during routine quality control procedures to highlight suspected anomalous regions. Supervised techniques [20]-[24] have been applied when a number of examples of different defects can be collected and can be used to train classifiers to model different behaviors of the signals observed. On the other hand, unsupervised techniques [25] have been proposed when examples are not available. In this case clustering techniques aggregate similar data, separating clusters whose signals belong to anomalous situations from those of sound areas. In a similar way, automatic seeded region growing approaches can be used to identify the debonding defects of different structures inspected by infrared thermography [26].

The performance of automatic systems for defect characterization not only depends on the informative content of input signals, but also on the architecture of the selected classifiers and the way they are trained with proper examples. The selection of the classifier parameters [25] and of thresholds in image preprocessing [26] can greatly impact on the final defect detection results.

In this paper, a signal processing technique based on a FIR filter and on an exponential model approximation has been designed to modify thermal signals reducing the effect of noise, and to enhance discrimination among signals produced by sound or defective regions. Then, a supervised classifier based on a decision forest [20] has been used to model defect discontinuities and at the same time to characterize their depths. The whole framework, made of preprocessing and classification phases, has been applied to a carbon laminate with several buried defects, demonstrating the validity of the proposed method. The paper is organized as follows: Section II discusses the signal processing technique and the classification methodology; Section III presents the dataset and the classification results. Final comments and remarks are in Section IV.

## 2. Methodology

The proposed methodology aims at investigating laminates made of carbon fiber reinforced polymer (CFRP) by means of pulsed thermography. The investigation will result in the characterization of the composite quality, i.e. in the identification of possible defects and their localization in depth. The next subsections will describe the whole pipeline for signal processing: the analytical model used to approximate heat transfer phenomena in defective media, the novel application of FIR filter to the input thermal signal, and the final classifier aimed to defect characterization.

### 2.1. Pulsed thermography and analytical model

The proposed methodology for defect characterization processes data obtained by optical pulsed thermography.

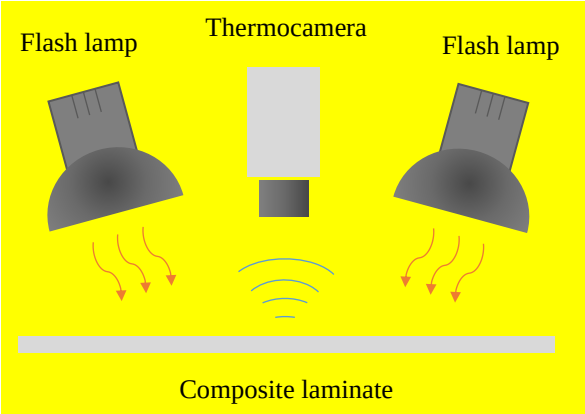


*Figure 1 - Sketch of a setup of optical pulsed thermography for inspection of composite laminates*

With reference to Figure 1, the inspected materials are illuminated by a heating pulse produced by high power optical sources. Source redundancy can be exploited to generate a uniform heat distribution on the surface of the composite laminate. As the heating pulse vanishes, the surface temperatures decrease uniformly on areas without internal defects, while, in presence of internal anomalies, a temperature pattern is produced on the sample surface. The shape of this pattern can be linked to the geometrical properties of the related defects in the three dimensions.

The dynamic behavior of the sample can be captured by an infrared camera, whose pixels sample the thermal decay of the surface temperature. Consequently, input data combine both spatial and temporal information in thermal videos, whose frames are maps of the surface temperature at a specific time instant, after the application of the input pulse.

As known [27], the presence of a defect at depth $d$ alters the temperature decay at the surface $T(t)$, whose analytical formulation is:

$$T(t) = \frac{Q}{\sqrt{\pi \rho c k t}} \left[ 1 + 2 \sum_{n=1}^{\infty} R^n \exp\left( -n^2 \frac{d^2}{\alpha t} \right) \right] \quad (1)$$

where $\rho$ is the mass density, $c$ is the heat capacity, $k$ is the thermal conductivity, $\alpha$ is the thermal diffusivity, $Q$ is the source energy transferred to the surface and $R$ is the reflection coefficient of the discontinuity.

In this case, thermal decays correspond to single profiles extracted from each pixel of the input thermal maps. These decays are individually processed to enhance reciprocal alterations and, thus, to aid the final classification of the corresponding surface regions. The main steps of this initial processing phase are the following ones [20]:

1. Input normalization: thermal dynamics are processed to be limited within [0,1] in order to compare profiles on the same reference scale. This task is easily reached by applying linear formulations to change the current range, bounded by its maximum and minimum values, to the target range between 0 and the unity.
2. Computation of the reference profile: the final goal of this processing is the enhancement of differences between thermal decays of a sound region and those of a defective one. For this reason, all surface profiles have to be further normalized to a reference profile which describe the thermal decay without discontinuities. This task is achieved by selecting a trust area of homogeneity from the sample under testing or from a reference pristine master. This region will represent the expected thermal behavior of a sound region. If it is not possible to select this area (or a pristine master), an extended region can be used, under the assumption that defects are well localized and much smaller than the area of the selected region. These thermal decays can be averaged to describe, with enough accuracy, the expected temperature of a sound region.
3. Normalized contrast computation: the input normalized thermal decay, obtained from the specific pixel, i.e. surface point, under testing, and the reference one are

compared to produce the normalized contrast. This profile ($\Delta T(t)$) is easily obtained by subtracting the reference temperature profile to the normalized input ones under analysis.

It is important to underline that normalized contrast computation can suffer from non-uniform heating of the composite laminates. Although tests have to be performed with the best source arrangement, it is difficult to achieve uniform heating over extended trust patches. In this case, temperature decays show the same behavior, since no discontinuities are in the trust area (or in the pristine master), but with relative delays. Several reference temperature profiles can thus be computed from a single trust area, by separating regions which have the same temperature at a specific time instant, i.e. along isothermal lines of the thermal map. Temperature contrasts will be thus normalized by taking into account the corresponding references, which depend on their position on the thermal map.

Every normalized temperature contrast, obtained at the end of the proposed flow, shows a characteristic behavior. The absence of any discontinuity under the surface of the sample produces a $\Delta T(t)$ profile constantly equal to 0, as effect of the difference with the expected behavior of the sound region. On the contrary, in case of subsurface defects, $\Delta T(t)$ profiles have the behavior reported in Figure 2, which displays the normalized input contrasts expected for different depths of the defects.

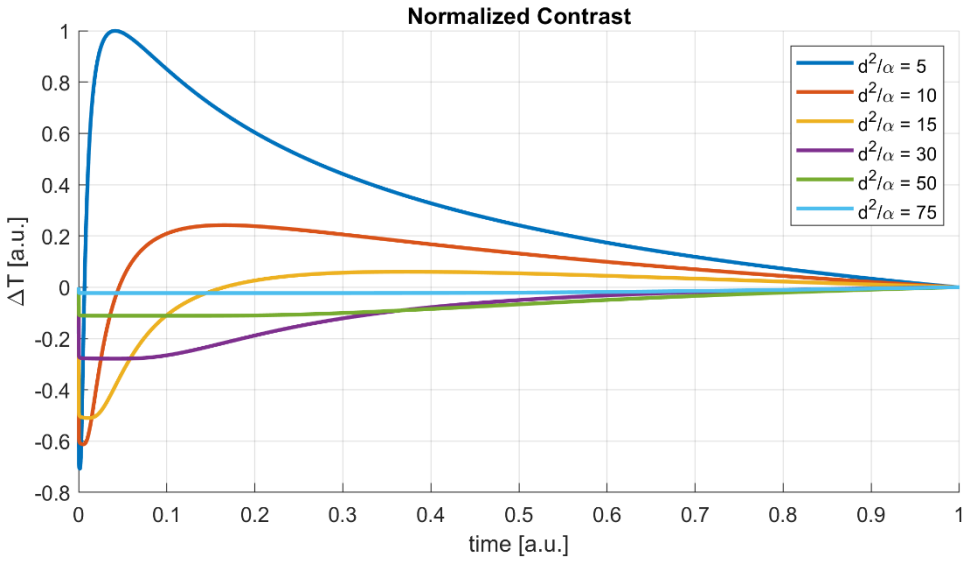


*Figure 2 - Analytical normalized thermal contrasts for different defect depths from surface (dark blue) to deep defects (light blue).*

These profiles own the following properties:

- At t = 0, $\Delta T(0) = 0$. This is consequence of the initial normalization of thermal decays. In all cases, with and without subsurface defects, the first sample of the acquired thermal decays is at the highest temperature and thus shifted to 1;
- At $t < t_d$, $\Delta T(t)$ rapidly varies with positive or negative derivatives depending on the position in depth of the discontinuity. It is worth noticing that the time constant $t_d$ determines the transition between two operating regimes and it is directly dependent on the depth of the defect, as well;
- At $t > t_d$, $\Delta T(t)$ follows an exponential decay till the limit of $\Delta T(t \rightarrow \infty) = 0$.

All properties can be represented by an exponential model made of three unknowns, whose values can be determined solving an optimization (fitting) problem in the least-square sense:

$$\Delta T_{approx}(t) = \left(a_1 t^2 + a_2 t\right)\exp\left(-a_3 t\right) \tag{2}$$

An example of the application of the model of Eq. (2) on the profiles of Figure 2 is reported in Figure 3.

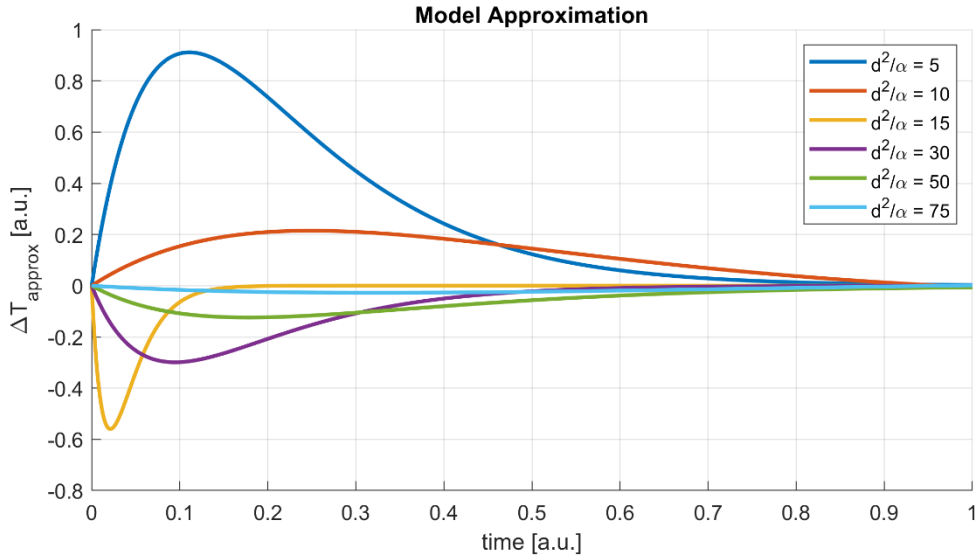


*Figure 3 - Results of the application of the model in Eq. (2) on the profiles in Figure 2.*

A generic normalized thermal contrasts, obtained inspecting the p-th pixel, is efficiently approximated by a feature vector $[a_1, a_2, a_3]_p$. The re-arrangement of all feature vectors on the corresponding position of the p-th pixel creates three spatial maps, one for each feature, which compress the whole information given by the thermal videos. The classification of surface regions in pristine of defective classes will be thus computed on only three input matrices of high informative contents.

Although this representation is very efficient, normalized temperature contrasts captured by the thermal camera are mostly affected by measurement noise. As a consequence, the discrimination between signals acquired from sound and defective regions can be hard if signal processing strategies are not adopted.

## 2.2. FIR filter design

The main novelty of the proposed methodology resides in the design of a FIR filter able to remove noise from input signals, thus improving discrimination among the different thermal behaviors.

As effect of measurement noise, input temperature contrasts highly fluctuate around their actual values. Preliminary experiments performed on regions of homogeneity, whose thermal contrast would be constantly equal to 0, demonstrate that the standard deviation of the mean thermal contrast, computed among profiles of sound regions, is equal to the 19.9% of the whole dynamics of this mean profile ($2.359 \times 10^{-3}$ over $11.814 \times 10^{-3}$, respectively). Noise reduction is mandatory to improve discriminations between profiles corresponding to defective or sound regions.

With this aim, a Finite Impulse Response (FIR) filter has been designed to properly cut off high frequencies, which carry the noise contribution. Starting from the characteristic values of the noise dynamics, the FIR filter has been designed with pass-band and stop-band frequencies at an angular frequency of 0.06 and 0.1, respectively, with pass-band ripple bounded within the limit of 0.05 and stop-band attenuation of $10^{-4}$. Following the Parks-McClellan algorithm for filter design [28], the optimal order for the equiripple FIR filter has been set to 135. These specifications produce the result in Figure 4, which reports the magnitude of the low-pass filter.

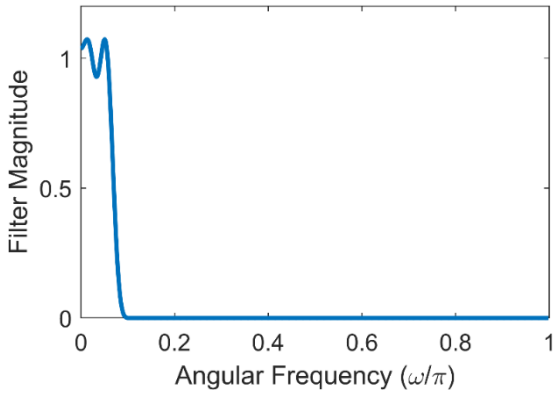


*Figure 4 - Magnitude of the low-pass FIR filter used to process input thermal contrasts.*

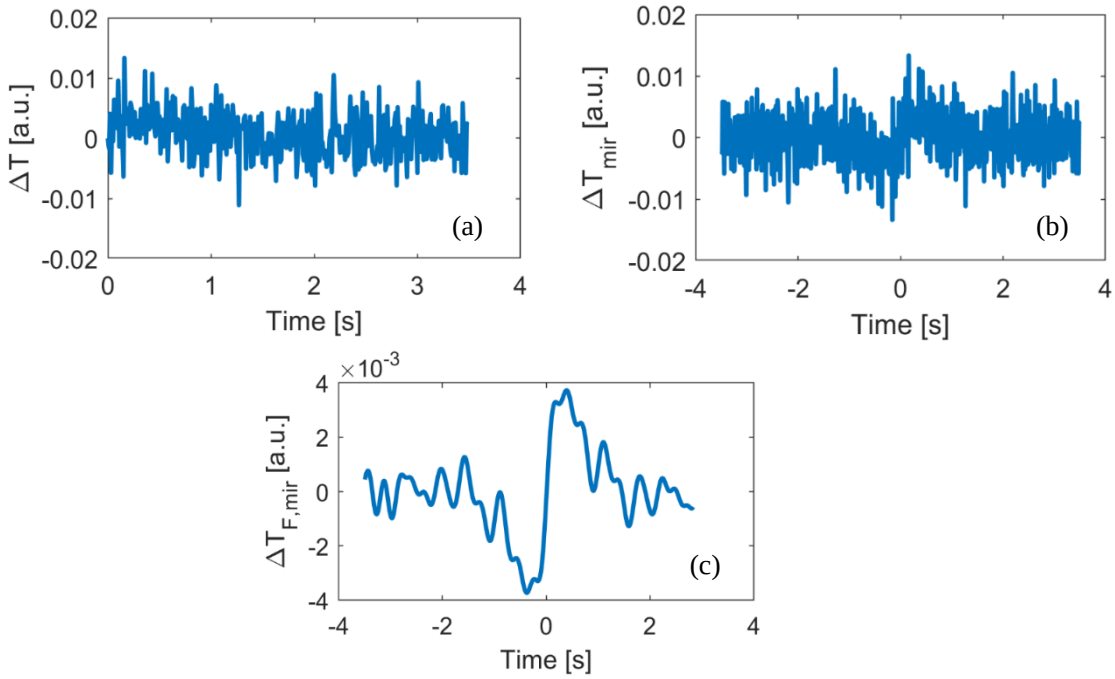


*Figure 5 - (a) Input thermal contrast with measurement noise and (b) corresponding mirrored signal. (c) Result of the filter on the mirrored input contrast.*

The application of a FIR filter to a signal requires a transient time interval before the effective operation (steady state). During this transient response, whose duration is equal to 134 time samples, the filter output can differ significantly from the expected value. In addition, the transient response clearly affects mainly the first range of samples of the

normalized temperature contrast, which carries most of the information. For this reason, the input signals, such as the one of Figure 5(a), are processed exploiting their properties. Since in pulsed thermography the temperature profiles are collected during the cooling phase, the first sample of the surface temperature always corresponds to the highest. When normalization is applied, this sample always becomes equal to 1. Consequently, the first sample of the temperature contrast, which is computed by subtracting the actual profile from the reference, vanishes. As the first sample of $\Delta T$ is always equal to zero, it is possible to mirror this signal for the negative part of the time domain. It creates an odd function, having symmetry around the origin, such as the one of Figure 5(b). Since the duplicated signal has a length $(2 \cdot n_T - 1)$ typically much higher than 134 (transient duration) and the expected behavior around the origin is almost linear, the FIR filter can effectively reach the steady-state in the range of interest (at $t > 0$). The results of the application of the FIR filter to the mirrored profile of Figure 5(b) are in Figure 5(c). This signal can thus be windowed in the range $[0, n_T - 1]$ to select the area of interest.

As an example, Figure 6 displays the results of the FIR filter on three signals belonging to areas with discontinuities placed at different depths. The application of the filter clearly improves the discrimination among the profiles, which are qualitatively distinctive of the properties of the corresponding defects. Then, these filtered normalized contrasts $\Delta T_F$ can be used to determine the three unknowns (features) of the exponential model of Eq. (2).

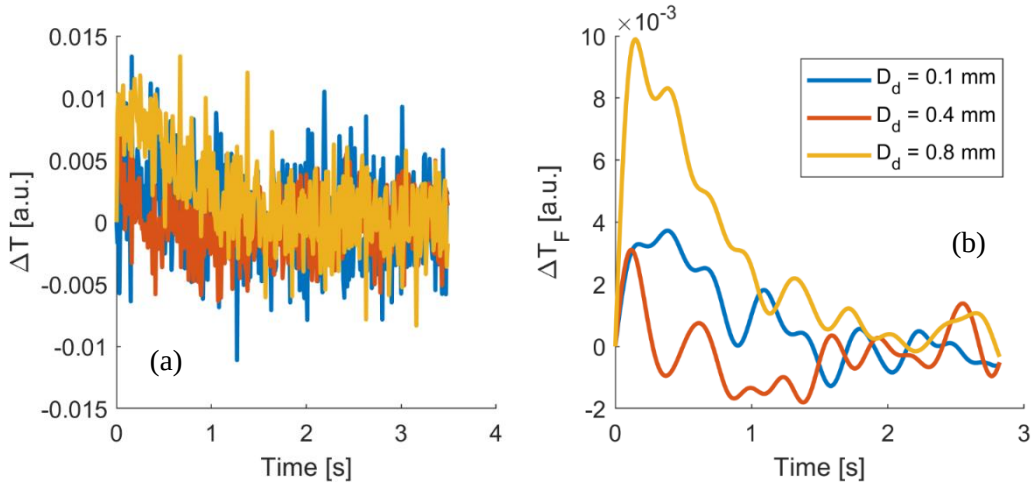


*Figure 6 - (a) Input thermal contrast from three actual regions having discontinuities at different depths and (b) corresponding results of the filtering process, which improves discrimination among signals. Yellow curves are taken from regions having the highest discontinuity (close to the surface), while red curves are from regions with the deepest one. $D_d$ is the depth of the discontinuity.*

## 2.3. Classifier

Every pixel of the images of a thermal video captured by a thermocamera produces a signal, which is processed and then approximated by the exponential model of Eq. (2). It produces three different maps (feature maps) having the same size of the thermal images, filled by the features [$a_1$, $a_2$, $a_3$] of the model. Hereafter, [$a_1$, $a_2$, $a_3$] label the unknowns of the model without the application of the FIR filter, whereas [$a_{1F}$, $a_{2F}$, $a_{3F}$] refers to the features of the filtered normalized thermal contrasts.

In both cases, feature vectors become the input of a classifier, which can state whether a pixel belongs to a defective region. Actually, the aim of this methodology is not only the recognition of the defect, but also its characterization in terms of depth. For this reason, the classifier will group pixels into three different classes, which are representative of the

position in depth of a detected defect. These groups are labeled as: (i) class 0 of sound regions; (ii) class 1 of surface, but buried, defects; (iii) class 2 of in-depth defects. Class 2 will be made of only defects at a specific depth. Then the classifier will generalize and label as class 2 all feature vectors from defects at similar depths, whose thermal behavior are comparable to the ones due to defects of class 2.

The classification is performed using a supervised learning approach. Several examples of the three classes of interest feed the classifier which is trained to recognize similar behaviors in the unknown inputs proposed during the testing phase. In this case the classifier is an ensemble of decision trees (decision forest). In particular, a decision forest of 30 trees [29] is used since it produces the best results with respect to a simple decision tree and k-NN algorithms [20]. With more details, a decision forest labels a set of input features following a voting mechanism. Every tree of the ensemble is a graph-based classifier performing a sequence of decisions. Then, the outputs are collected to select the best prediction on that input features. The cooperation of different trees improves the robustness of the classifier in response to minor alterations of the inputs.

A comparative investigation will be performed by changing the size of the input vectors which feed the classifier. Specifically, for each pixel of the surface, the feature maps made of the values of [$a_1$, $a_2$, $a_3$] and [$a_{1F}$, $a_{2F}$, $a_{3F}$] will be windowed by square masks of different sizes ($Q \times Q$, $Q$ = 1, 3, 5, …), centered on the pixel under analysis. If the pixel under analysis is close to the image boundary, so that the window is off of the image edges, border replication is used to fill the feature entries outside the image, but within the square mask. The resulting values of the masking process will be then reshaped in vectors of size of $(3 \cdot Q \cdot Q) \times 1$. These sets of features will be the actual inputs to the

classifier and, depending on their sizes, will add increasing neighborhoods in the final classification performed by the decision forest.

## 3. Experiments and Results

The ability of the proposed FIR-aided methodology in the classification of defects will be tested on an actual sample of a CFRP laminate, filled by both surface and in-depth inclusions of foreign materials. The next subsections will discuss on classification results, showing the main advantages given by the use of the FIR filter in the preliminary processing of the normalized temperature contrasts.

### 3.1. Input dataset

Experiments have been performed on a sample laminate of CFRP made of eight layers of unidirectional carbon fiber (layer thickness of 0.1 *mm*) [20]. The specimen has been enriched during production with several inclusions of foreign materials, in order to generate known defects at different depths. Although these defects belong to a specific category, namely inclusions, the proposed method can be used to detect any other kind of defects, once examples are provided during training. Following the principles of supervised learning, these examples will represent the thermal behavior expected for that specific defect. In a similar manner, the classifier can be also trained with more examples representing the thermal behavior of defects placed at other depths than the one of class 2. In this way, further classes of in-depth defects can be recognized, thus reaching higher accuracy in depth estimation.

With reference to the sketch in Figure 7, four foreign objects of white paper and fluorinated ethylene propylene (FEP) are placed in the laminate: two of them are surface defects (class 1) placed between the two last layers; the other two objects are in-depth

defects, between the fourth and the fifth layers (class 2). These four objects are made of 0.08-mm-thick white paper (see the two white blocks in Figure 7) and 0.05-mm-thick fluorinated ethylene propylene (FEP, see the two purple blocks in Figure 7). Their in-plane sizes are alternatively equal to 5×5 mm and 25×25 mm. These defects have been chosen in agreement with both the geometrical tolerances of aeronautical production lines, and the capability of IR thermography in inspecting defects of small sizes at high depths.

The sample is inspected by dividing its surface in three different regions, whose extension is related to the field-of-view of the thermocamera used for experiments (FLIR X6540sc [30]). One region trains the decision forest, and the other two regions test its performance. The two test regions have an overlap area with a surface defect of FEP. The remaining part of the test region 2 encloses a homogeneous region (class 0). However, this area is highly structured and the corresponding thermal behavior is similar to the one of defective regions. Consequently, this further test will state the capability of the method in discriminating actual defects from buried structures due to the specific layup of the composite laminate.

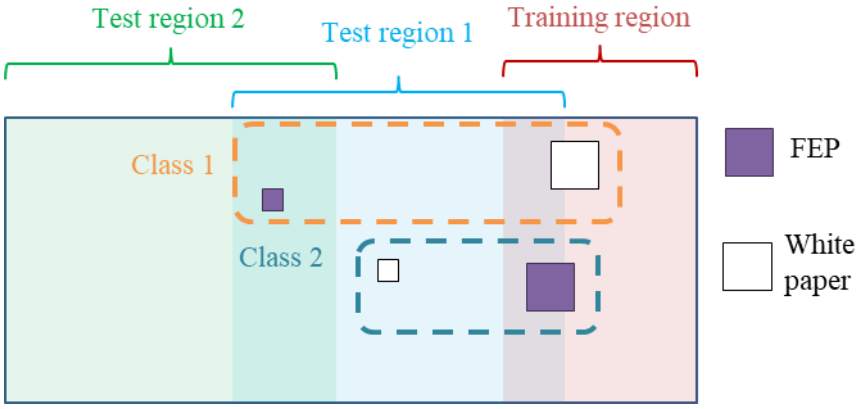


*Figure 7 - Sketch of the sample laminate, detailed in three different regions. Defects are represented by squares; the remaining area refers to sound material. Sizes are reported in scale.*

The proposed methodology requires the first selection of a trust region without defects, which will be used to create the reference thermal decay of a pristine region. This reference is mandatory for the final computation of the normalized thermal contrast $\Delta T(t)$, which will be further approximated by the exponential model. Since the training region is supposed to be completely known in terms of its geometry, the extended trust region has been selected as the rectangular area made of the last 75 columns of the training region (see the right side of the sample sketched in Figure 7).

## 3.2. FIR filter application

The use of the FIR filter is aimed to the reduction of measurement noise and to the consequent enhancement of discrimination between thermal decays produced by pristine and defective regions. These results can be highlighted by displaying the feature maps before and after the application of the FIR filter (see the left and right columns of Figure 8, which are related to the three regions of interest). In this case, each channel of the false color maps represents the contribution of a single feature of the exponential model.

These images represent the input for the actual classification. Each image will be windowed by square masks to create the input vectors. Under these hypotheses, it is easy to understand that an improvement of map contrast will produce better results, since discrimination will be enhanced.

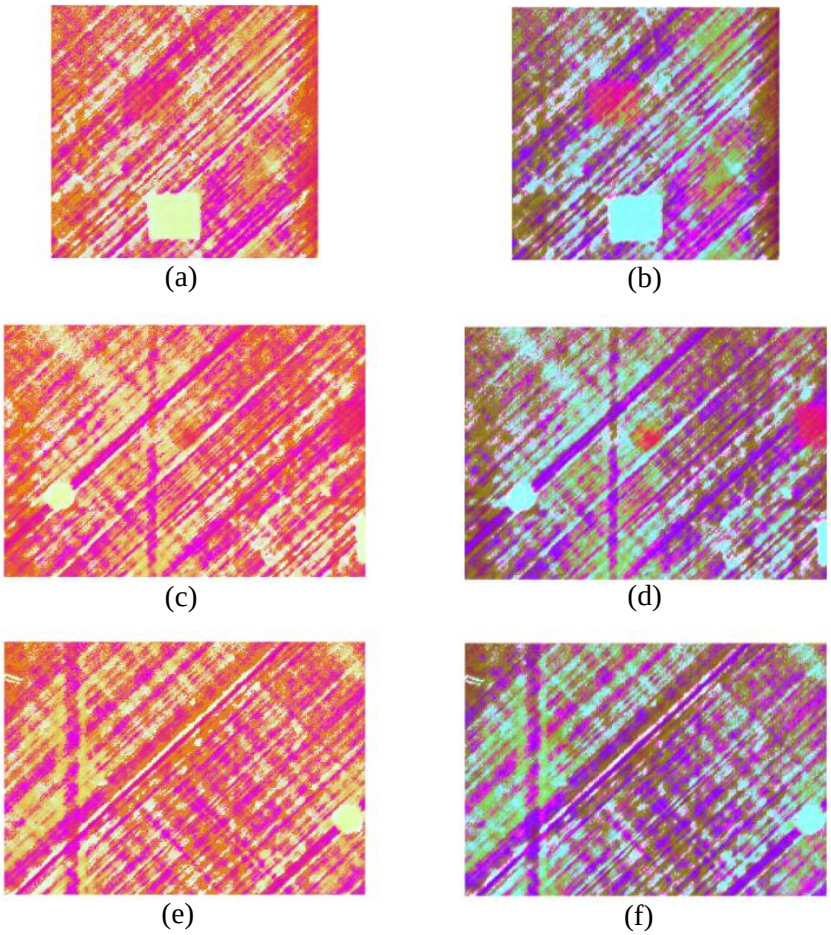


*Figure 8 - Images in false colors from the inspection of: (a)-(b) the training region and (c)-(f) of the test regions. Each RGB channel represents a feature of the exponential model before (left column) and after (right column) the FIR filter.*

As expected, a qualitative insight on these results proves that the use of the FIR filter on the input normalized thermal contrasts improves the image contrast: defects of class 2 are enhanced with respect to the background (sound region).

Quantitatively, the improvement of image contrast can be viewed by inspecting the image entropy. This value measures the energy of a gray-scale image, in terms of its randomness or its textures [31]. Specifically, high value of entropy refers to a high level of details within the image, whose pixels' amplitudes vary with high variance (high image contrast). On the contrary, if the level of the entropy is low, the image has few details and low contrast, thus reducing the final capability of the classifier to discriminate among classes.

The feature maps are made of three channels. For this reason, the whole entropy is computed by averaging the three entropy values of each channel. These results, obtained for the six images of Figure 8, are reported in Table 1.

*Table 1 - Average values of per-channel entropy of the input feature maps of the three regions under analysis, with or without the application of the FIR filter*

| **Region** | **Before FIR filter** | **After FIR filter** |
|---|---|---|
| Training | 10.166 | 11.042 |
| Test 1 | 10.369 | 10.872 |
| Test 2 | 10.169 | 11.276 |

The analysis of the results in Table 1 confirms the qualitative outcomes of the inspection of Figure 8. Specifically, the entropy of the feature maps of the training region, and the test regions 1 and 2 increases of 8.62%, 4.86% and 10.88%, respectively. This clearly proves that the application of the FIR filter increases the number of details within the feature maps.

It is important to notice that the gain in the image contrast is unambiguously due to an improvement of the contrast between defective and sound regions. At the same time, also

the amplitude magnification of the texture of the normalize input contrast has effects on the increase of whole entropy. Both contributions are proposed to the input layer of the classifiers, which will manage properly the enhanced contrasts to produce better results.

### 3.3. Classification results

Classification is performed considering different sizes of the mask used to create the informative input vectors. The mask sizes ($Q \times Q$) are set to 1×1 (scalar input), 3×3, 5×5 and 7×7. Final classifications have been achieved by training four decision forests depending on the size of the masks. As a consequence, all results to be shown in the next lines are obtained under the best working conditions for each size considered to window input feature maps.

The performance of the classifier will be expressed in terms of precision and recall [32]. In standard two-class classification problems, precision states whether predictions of a class are true, whereas recall is related to the number of missed predictions of that class. When multi-class problems are tackled, precision and recall metrics can still have the same meaning, but refers to the comparison of a specific class with respect to the others.

As a first step, it is important to determine which mask size gives the best result in the classification of the surface pixels. For this reason, Figure 9 reports the average precision and recall, computed on class 1 and 2 (defective) against the others by weighting their influence by the population of the corresponding classes.

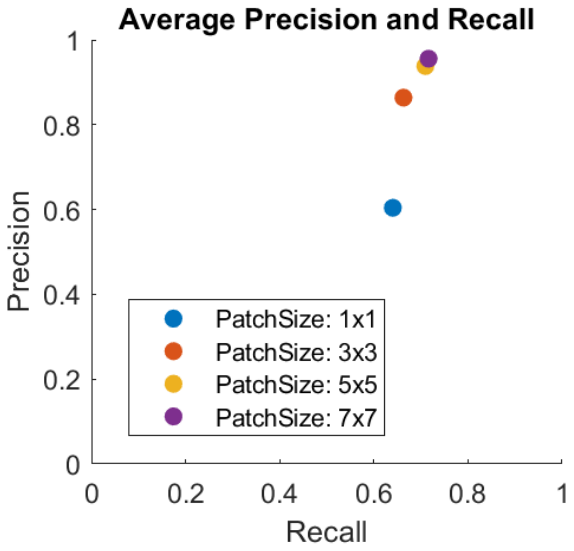


*Figure 9 - Average precision and recall for the detection of defects against sound regions*

Figure 9 clearly demonstrates that increasing the size of the feature vectors, including more neighborhoods, i.e. information, improves the results, which approach the up-right corners of the plots (both average precision and recall are close to unity).

As a second step, a comparison of results before ($[a_1, a_2, a_3]$) and after ($[a_{1F}, a_{2F}, a_{3F}]$) the application of the FIR filter have been performed in terms of precision and recall of each of the three classes against the remaining, by considering a size of the square mask of 7×7. These results are shown in Table 2.

*Table 2 - Precision and Recall before and after the application of the FIR filter*

| | **Metrics** | **0 vs All** | **1 vs All** | **2 vs All** |
|---|---|---|---|---|
| **Before FIR filter** | Precision | 0.9915 | 0.9967 | 0.9112 |
| | Recall | 0.9994 | 0.521 | 0.7312 |
| **After FIR filter** | Precision | 0.9936 | 0.9932 | 0.9134 |
| | Recall | 0.9992 | 0.7189 | 0.7355 |

As a first point, it is important to notice that recall results for defects of class 1 are relatively low, although the inspection of Figure 8 reveals that surface defects are well contrasted in the feature maps, both before and after the use of the FIR filter. This results from the presence of the internal structures of the laminate, due to its layup. All these textured regions are grouped in class 0. The classifier is thus trained to model class 0 in order to include also these textures, which can also cross defects of class 1. As a consequence, both class 0 and 1 can overlie in the same point and, even though input features are well separated, the classifier is not able to discriminate between class 0 and 1: observations of class 1 can be labeled as class 0, downing the estimated recall in Table 2.

Moreover, the comparison of results before and after the application of the FIR filter shows that precision values are almost equal. On the contrary, the recall value computed for class 1 against class 0 and 2 increases of about 19.8%. It means that missed predictions of defects of class 1 are significantly reduced, i.e. surface defects are better recognized over the sample laminate. This is effect of the contrast enhancement shown by the inspection of Figure 8, which implicates an improvement of discrimination between thermal signals produced by sound regions and defective ones. This improvement is of great importance in the field of aeronautics, where defects must be recognized with the best reliability for safety reasons.

The application of the proposed methodology on training and test regions is displayed in Figure 10. In this case, classes are labelled with different colors: dark blue corresponds

to sound regions (class 0), whereas light blue and yellow refer to class 1 and 2, respectively.

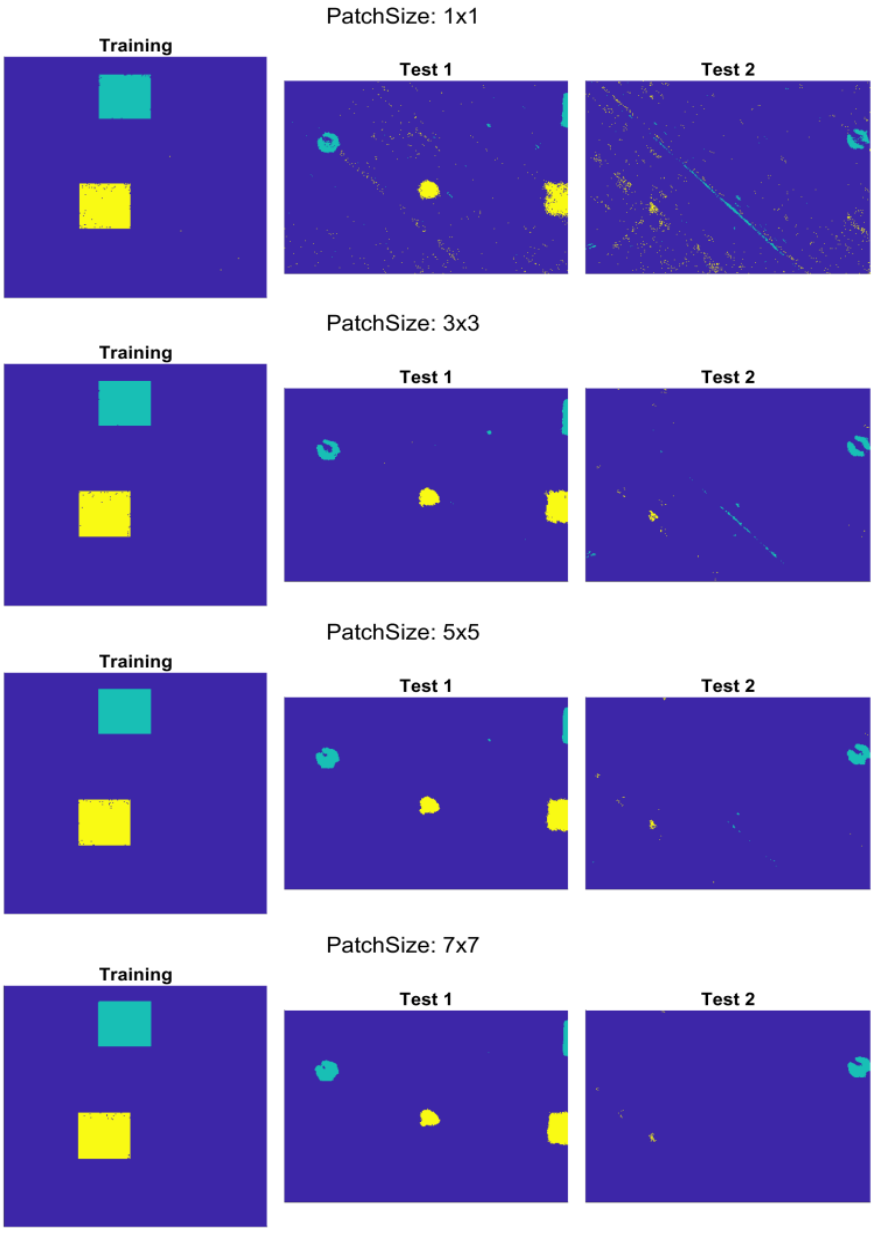


*Figure 10 - Results of classification changing the size of the patches used to define input features. Dark blue refers to class 0 (homogeneous regions); cyan and yellow indicate the defective classes (1 and 2 respectively).*

The inspection of Figure 10 proves the capability of the proposed methodology also in the reduction of false positives, i.e. wrong assignments of pixels of sound regions to defective classes, as the number of neighborhoods involved in the classification increases. In particular, a patch size equal to 7×7 gives the best results, especially in test region 2, which is mostly filled by sound regions with buried structures due to the specimen layup. Missed predictions of defects of class 1 in the test region 2, which down the recall value of class 1 vs All in Table 2, are also limited by increasing the patch size to 7×7.

The quality of these results is also confirmed comparing the outputs of Figure 10 with the result of [20]. The application of the FIR filter significantly downs the presence of spots labeled as internal defects, but actually due to the pattern of the specimen layers. These wrong assignments are removed without improving the training phase, i.e. without including more samples of the class 0 in order to better characterize its behavior. It clearly proves that the FIR filter maximizes the ability of the classifier to group all regions different from the ones of class 1 and 2 into the cluster made of points of class 0. This outcome can be measured in terms of the average precision of the defective classes, computed by weighting their influence by the population of the corresponding classes. If the comparison is performed on output obtained with 7×7 square patches, the use of the FIR filter on normalized thermal contrasts increases the average precision value in [20] from 92.21% to 95.56%.

## 4. Conclusions

This paper describes a methodology for automatic defect classification in composite laminates inspected by pulsed thermography. A FIR filter has been designed to process input thermal signals and reduce measurement noise. It leads to higher discrimination

among signals captured from regions with or without defects. A classifier, based on a decision forest of 30 trees, processes input signals, approximated by an exponential model, in order to distinguish the properties of the defects in terms of their depths. Experimental analyses, performed on an actual CFRP laminate with four defects (inclusions) of two classes (surface and in-depth defects), demonstrates the reduction of false negatives, as a consequence of the application of the FIR filter on the input thermal signals. Also wrong assignments of pixels of homogeneity to defective classes decrease, as the number of neighborhoods involved in the classification increases to 7×7. Future work will be aimed to prove the ability of the proposed method to generalize the characterization of defects on other samples, made of different constitutive media or arrangement of layers.

## Acknowledgements

This work is part of the Italian MIUR Project DITECO (Ref. PACPON03PE_00067_2). The authors would like to thank Mr. Michele Attolico and Mr. Giuseppe Bono for their fundamental contributions, and Mr. Pasquale Cavallo for the experimental activity performed in this work.

## References

[1] Nikishkov Y, Airoldi L, Makeev A. Measurement of voids in composites by X-ray Computed Tomography. Composites Science and Technology, 2013, 89:89-97.

[2] Hassen AA, Taheri H, Vaidya UK. Non-destructive investigation of thermoplastic reinforced composites. Composites Part B: Engineering, 2016, 97:244-254.

[3] Hosur MV, Murthy CRL, Ramamurthy TS, Shet A. Estimation of impact-induced damage in CFRP laminates through ultrasonic imaging. NDT&E International, 1998, 31(5):359-374.

[4] Tamborrino R, Palumbo D, Galietti U, Aversa P, Chiozzi S, Luprano VAM. Assessment of the effect of defects on mechanical properties of adhesive bonded joints by using non destructive methods. Composites Part B, 2016, 91:337-345.

[5] Castellano A, Fraddosio A, Piccioni MD. Ultrasonic goniometric immersion tests for the characterization of fatigue post-LVI damage induced anisotropy superimposed to the constitutive anisotropy of polymer composites. Composites Part B: Engineering, 2017, 116:122-136.

[6] De Angelis G, Meo M, Almond DP, Pickering SG, Angioni SL. A new technique to detect defect size and depth in composite structures using digital shearography and unconstrained optimization. NDT&E International, 2012, 45:91-96.

[7] Pérez MA, Gil L, Oller S. Impact damage identification in composite laminates using vibration testing. Composite Structures, 2014, 108:267-276.

[8] Angelidis N, Irving PE. Detection of impact damage in CFRP laminates by means of electrical potential techniques. Composites Science and Technology, 2007, 67:594-604.

[9] Shepard S. Advances in pulsed thermography. Proceedings of SPIE, Thermosense-XXIII, 2001, 4320:511

[10] Palumbo D, De Finis R, Demelio GP, Galietti U. Study of damage evolution in composite materials based on the Thermoelastic Phase Analysis (TPA) method. Composite Part B, 2017, 117:49-60.

[11] Stone DEW, Clarke B. Ultrasonic attenuation as a measure of void content in carbon-fibre reinforced plastics. Non-Destructive Testing, 1975, 8(3):137-145.

[12] Garnier C, Pastor ML, Eyma, F, Lorrain B. The detection of aeronautical defects in situ on composite structures using Non Destructive Testing. Composite structures, 2011, 93(5):1328-1336.

[13] Vavilov VP, Burleigh DD. Review of pulsed thermal NDT: Physical principles, theory and data processing. NDT&E International, 2015, 73:28-52.

[14] Mayra G, Stocknera G, Plassera H, Hendorfera G, Burgholze P. Parameter estimation from pulsed thermography data using the virtual wave concept. NDT&E International, 2018, 100:101-107.

[15] Wang Z, Tian GY, Meo M, Ciampa F. Image processing based quantitative damage evaluation in composites with long pulse thermography. NDT&E International 2018, 99:93-104.

[16] Almond DP, Angioni SL, Pickering SG. Long pulse excitation thermographic non-destructive evaluation. NDT&E International, 2017, 87:7-14.

[17] Balageas D, Roche JM. Common tools for quantitative time resolved pulse and step-heating thermography- part I: theoretical basis. QIRT Journal, 2014, 11:10-28.

[18] Palumbo D, Galietti U. Damage investigation in composite materials by means of new thermal data processing procedures. Strain, 2016, 52(4):276-285.

[19] Alvarez-Restrepo CA, Benitez-Restrepo HD, Tobon LE. Characterization of defects of pulsed thermography inspections by orthogonal polynomial decomposition. NDT&E International, 2017, 91:9-21.

[20] Marani R, Palumbo D, Renò V, Galietti U, Stella E, D'Orazio T. Modeling and Classification of Defects in CFRP Laminates by Thermal Non-Destructive Testing. Composites Part B: Engineering, 2018, 135:129-141.

[21] D'Orazio T, Leo M, Distante A, Guaragnella C, Pianese V, Cavaccini G. Automatic ultrasonic inspection for internal defect detection in composite materials. NDT&E International, 2008, 41(2):145-154.

[22] Leo M, Looney D, D'Orazio T, Mandic DP. Identification of defective areas in composite materials by bivariate EMD analysis of ultrasound. IEEE Transactions on Instrumentation and Measurement, 2012, 61(1):221-232.

[23] Darabi A, Maldague X. Neural network based defect detection and depth estimation in TNDE. NDT&E International, 2002, 35(3):165-175.

[24] D'Orazio T, Guaragnella C, Leo M, Spagnolo P. Defect detection in aircraft composites by using a neural approach in the analysis of thermographic images. NDT&E International, 2005, 38(8):665-673.

[25] Marani R, Palumbo D, Galietti U, Stella E, D'Orazio T. Automatic detection of subsurface defects in composite materials using thermography and unsupervised machine learning. In IEEE 8th International Conference on Intelligent Systems (IS), 2016, 516-521.

[26] Feng Q, Gao B, Lu P, Woo WL, Yang Y, Fan Y, Qiu X, Gu L. Automatic seeded region growing for thermography debonding detection of CFRP. NDT&E International 2018, 99:36-49.

[27] Almond DP, Patel PM, Photothermal science and techniques, Nederland: Springer; 1996.

[28] Rabiner LR, Gold B. Theory and application of digital signal processing. Englewood Cliffs, New Jersey: Prentice-Hall; 1975.

[29] Kuncheva LI, Combining pattern classifiers: methods and algorithms. Hoboken, New Jersey: John Wiley & Sons; 2004.

[30] Online available: https://www.flir.com/browse/rd-and-science/high-performance-cameras/

[31] Gonzalez RC, Woods RE. Digital image processing. Upper Saddle River, New Jersey: Prentice-Hall; 2001.

[32] Olson DL, Delen D. Advanced Data Mining Techniques. Berlin Heidelberg: Springer-Verlag; 2008.